View metadata, citation and similar papers at core.ac.uk
brought to you by CORE
provided by Italian Group Fracture (IGF): E-Journals / Gruppo Italiano Frattura

J. Toribio et alii, Frattura ed Integrità Strutturale, 30 (2014) 40-47; DOI: 10.3221/IGF-ESIS.30.06

Focussed on: Fracture and Structural Integrity related Issues

Numerical analysis of hydrogen-assisted rolling-contact fatigue of wind turbine bearings

J. Toribio, M. Lorenzo, D. Vergara, V. Kharin
Fracture of Materials and Structural Integrity Research Group, University of Salamanca, Spain
toribio@usal.es, mlorenzo@usal.es, dvergara@usal.es, gatogris@usal.es

ABSTRACT. Offshore wind parks at locations further from the shore often involve serious difficulties, e.g. the maintenance. The bearings of offshore wind turbines are prone to suffer hydrogen-assisted rolling-contact fatigue (HA-RCF). Three important aspects linked with bearing failures are being extensively researched: (i) rolling contact fatigue (RCF), (ii) influence of carbide particles on fatigue life, and (iii) local microplastic strain accumulation via ratcheting. However, there is no reference related to bearing failure in harsh environment. This way, this paper helps to gain a better understanding of the influence of hydrogen on the service life of offshore wind turbine bearings through a numerical study. So, the widely used RCF ball-on-rod test was simulated by finite element method in order to obtain the stress-strain state inside the bearings during life in service and, from this, to elucidate the potential places where the hydrogen could be more harmful and, therefore, where the bearing material should be improved.

KEYWORDS. Hydrogen-assisted rolling-contact fatigue; Wind turbines; Bearings; Numerical analysis.

INTRODUCTION

Offshore wind farms reach higher levels of energy production than onshore installations. There are several reasons to this fact: (i) the wind turbine size does not have the usual onshore limitations related to road transportation or noise regulations, (ii) offshore wind speeds are considerably higher than onshore [1]. However, offshore wind parks present maintenance problems. The bearings of offshore wind turbines can suffer hydrogen-assisted rolling-contact fatigue (HA-RCF) due to: (i) the use of long-life lubricants with certain additives to extend the turbine maintenance intervals, what contributes to lubricant decomposition and hydrogen generation; (ii) the increased likelihood of moisture entering the bearing; (iii) the salty environment increases the corrosion of materials and hence the probability of hydrogen penetration.

Three important aspects linked with bearing failures are being extensively researched: (i) rolling contact fatigue (RCF) [2-5], (ii) influence of carbide particles on fatigue life [6,7], and (iii) local microplastic strain accumulation via ratcheting [8-10]. However, there is no literature related with bearing failures in harsh environment. This way, this paper helps to gain a better understanding of the influence of hydrogen on the life in service of offshore wind turbine bearings through a numerical study. So, the widely used RCF ball-on-rod test [10-13] was simulated by finite element method to obtain the stress-strain state of bearings during life in service and, from this, to elucidate the potential places where the hydrogen could be more harmful causing final catastrophic failure by hydrogen embrittlement (HE) related phenomena.

NUMERICAL MODELING

The study was divided into two uncoupled analysis. On one hand, the numerical simulation by means of a commercial finite element (FE) code was used for obtaining the stress and strain states after six revolutions of the bar. From the results of such an analysis, a simple estimation of the hydrogen accumulation for long time of exposure to hydrogenating environment was carried out allowing the estimation of the potential hydrogen damage places. The geometry analysed consist of a steel bar of length L= 6 mm and diameter d = 9.53 mm rotating in contact with three equidistant steel balls of diameter D = 12.70 mm and applying a point load of F = 300 N over the bar surface, as depicted in the scheme of Fig. 1a. The complete 3D geometry can be simplified to a half just considering the symmetry plane r-θ shown in Fig. 1b and applying the corresponding boundary conditions as restricted displacement on the bar axial direction for all the nodes placed inside the symmetry plane. Thus, an important save of computing time is achieved optimizing the available resources. In addition, the geometry of the contacting balls can be also simplified considering the symmetry plane r-z of such components. Taking this into account, only a quarter of the whole geometry is modelled, as seen in Fig. 1b.

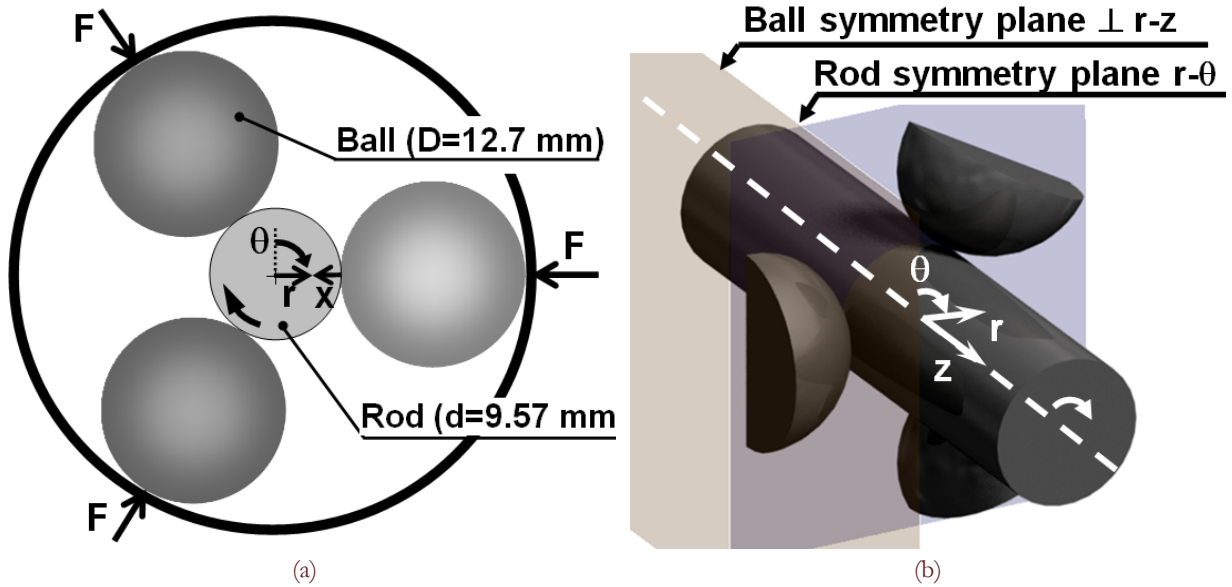

Figure 1: (a) Scheme of the analysed geometry for a ball-on-rod test and (b) 3D geometry.

The numerical modelling of the ball-on-rod test (six revolutions) was carried out by considering the material constitutive law to be elastic perfectly plastic corresponding to a steel with the following material properties for both rod and balls: Young modulus, E = 206 GPa, Poisson coefficient, ν= 0.3 and material yield stress σ_Y = 2065 MPa. The analysis was carried out with isotropic strain hardening of the material and updated Lagrange procedure. According to the Hertz theory considering only the elastic response of the components [14], a very localized effect can be expected in the contact zone between the rod and the balls. According to this, a ball pressuring a cylinder must undergo a contact pressure of 5.5 GPa with a elliptic contacting zone whose axis length are 160 μm and 231 μm respectively.

From results of the mechanical simulation, a simple estimation of the behavior against HE of the bar can be carried out considering that hydrogen diffusion proceeds from the bar surface to inner points as a function of the gradients of both hydrostatic stress (σ) and hydrogen solubility ($K_{s\varepsilon}$) [15-17]:

$$\mathbf{J} = -D(\bar{\varepsilon}_p)\left\{\nabla C - C\left[\frac{V_H}{RT}\nabla\sigma + \frac{\nabla K_{S\varepsilon}(\bar{\varepsilon}_p)}{K_{S\varepsilon}(\bar{\varepsilon}_p)}\right]\right\} \quad (1)$$

R being the universal gases constant, V_H the partial volume of hydrogen, T the absolute temperature and $K_{s\varepsilon}$ the hydrogen solubility that is itself a one-to-one monotonic increasing function of equivalent plastic strain, as explained in detail

elsewhere [15-17]. In particular, a linear relationship between plastic strain and solubility in the form $K_{S\varepsilon} = 1+4\varepsilon_p$ was considered to be adequate, cf. [15-17].
After using the matter conservation law and applying the Gauss-Ostrogradsky, the following second-order partial differential equation of hydrogen diffusion is obtained:

$$\frac{\partial C}{\partial t} = \nabla \cdot \left[D\nabla C - DC\left(\frac{V_H}{RT}\nabla\sigma + \frac{\nabla K_{S\varepsilon}(\bar{\varepsilon}_P)}{K_{S\varepsilon}(\bar{\varepsilon}_P)} \right) \right] \tag{2}$$

The equilibrium concentration of hydrogen for infinite time of exposure to harsh environment is the steady-state solution of the differential equation. It takes the form of a Maxwell-Boltzman distribution as follows:

$$C_{eq} = C_0 K_{S\varepsilon}(\bar{\varepsilon}_P) \exp\left[\frac{V_H}{RT}\nabla\sigma \right] \tag{3}$$

where C_0 is the equilibrium hydrogen concentration for the material free of stress and strain. According to previous equations, hydrogen diffusion is driven by: (i) the negative gradient of hydrogen concentration (in the classical Fick´s sense); (ii) the positive gradient of hydrostatic stress; (iii) the positive gradient of hydrogen solubility, the latter is one-to-one related to the gradient of equivalent plastic strain so that the plastic strain gradient (a continuum mechanics variable that appears as an output after the FE computation) can be analysed instead of the hydrogen solubility gradient.

MECHANICAL ANALYSIS: STRESS AND STRAIN

Numerical simulation allows the determination of the stress and strain state under cycling loading during the ball-on-rod test. Fig. 2a shows the global view of the distribution of von Mises stress in the steel rod and the contacting balls at the end of the sixth cycle (after passing three contacting balls) and Fig. 2b shows a detail view of the von Mises distribution at the contact of one of the balls.

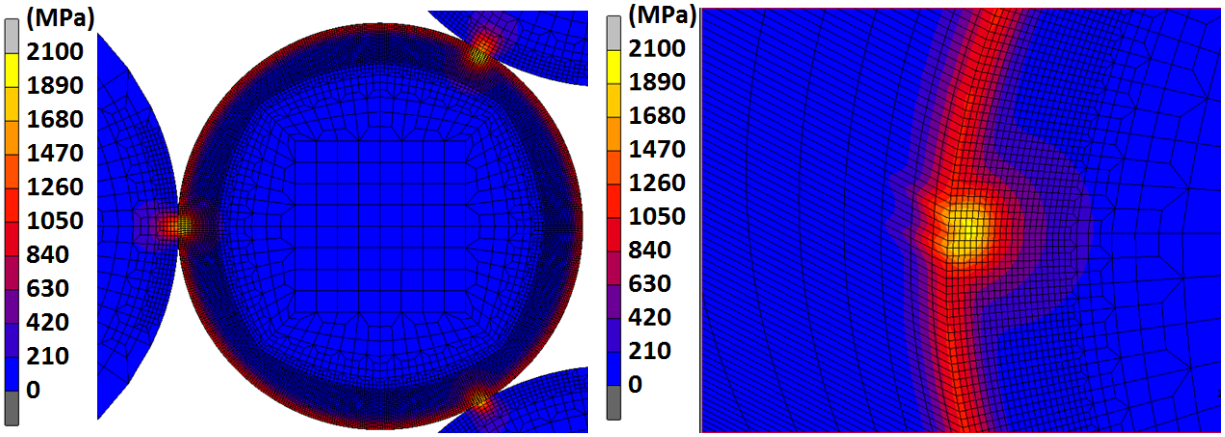

(a) (b)

Figure 2: Distribution of von Mises stress after the sixth loading cycle: (a) 2D view of the contacting plane and (b) 3D detail view at the contact of one of the balls.

Results shown in Fig. 2, reveal a heavy stress concentration localized at the contacting zones of each ball with the rolling rod. This effect progressively vanishes as the distance from the contact zone increases. Outside of the locally affected zone, the von Mises stress is homogenously distributed with a heavy stress concentration ring located at the vicinity of the rod surface. Within the stress concentration zone, the values of the von Mises stress reach the material yield stress what implies the appearance of plastic strains near the rod skin as will be discussed lately. For a more detailed analysis, the radial distribution for different values of the circunferential coordinate θ are represented in Fig. 3 considering the following sections: (i) θ = 45º, (ii) θ = 20º, (iii) θ = 10º, two planes placed close to the contacting ball (iv) θ = 5º, (v) θ = 2º and finaly (vi) θ = 0º representing the contact plane between one of the balls and the rod.

The radial stress distribution reveals the localized effect at the contact zone with the balls which is spread through a depth from the rod surface of about 1.5 mm reaching null values at the rod centre. At the contact radius ($\theta = 0^o$) the maximum stress is placed out of the rod surface for an approximate depth of 165 μm (reaching there the material yield stress) and, therefore, generating plastic strains at the surroundings of this place. The distribution for the other radius in contact with the other balls ($\theta = 120^o$ and $\theta = 240^o$) is equivalent to that shown in Fig. 3.

As a consequence of the values of the von Mises stress at the rod surface vicinity, plastic strains are distributed through such a zone. Fig. 4 shows the 3D view of the field of equivalent (cumulative) plastic strain after the six cycle of the test was completed and the radial distribution of such a variable is plotted in Fig. 5. In the same way, Fig. 6 shows the 3D view of the field of hydrostatic stress after the sixth cycle of the test was completed and Fig. 7 shows the radial distribution of such a variable for diverse values of θ.

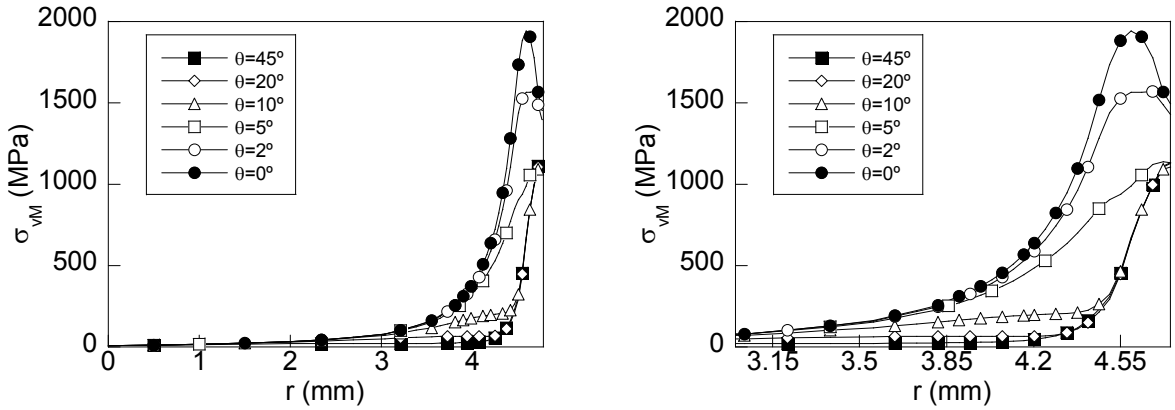

Figure 3: Radial distribution of von Misses stress for diverse circumferential coordinate θ: (a) general plot and (b) detail plot near the rod surface (zone with strong gradients).

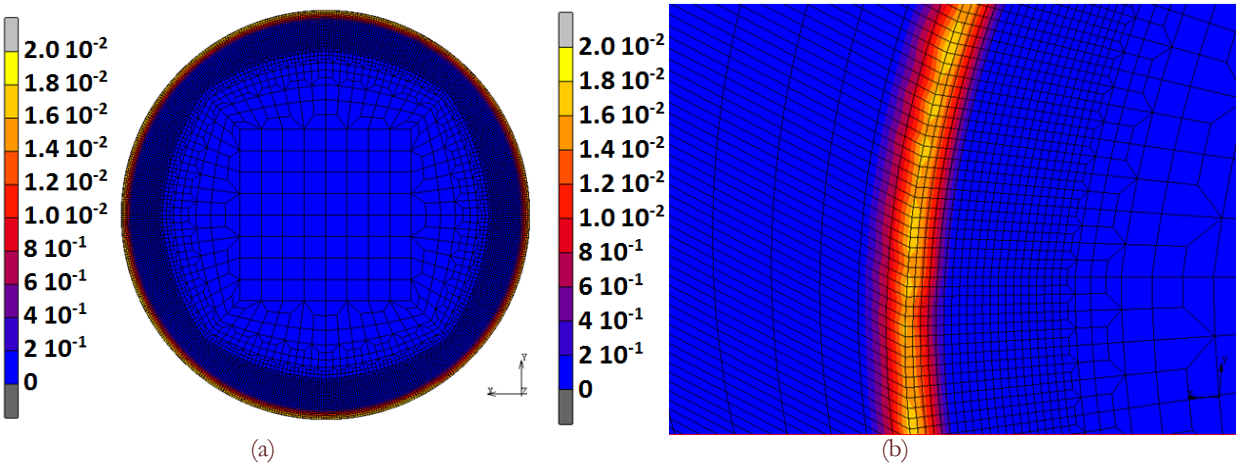

Figure 4: Field of equivalent (cumulative) plastic strain on the cylinder after six cycles of the ball-on-rod test. (a) 2D view of the contacting plane and (b) 3D detail view at the contact of one of the balls.

The first driving force for hydrogen diffusion, the gradient of equivalent plastic strain, is negative and only affects the plastic strain ring near the rod surface (Fig. 5). With regard to the second driving force for hydrogen diffusion, the gradient of hydrostatic stress, at the contact plane ($\theta = 0^o$) a compressive nature distribution in radial direction of such a variable is obtained, progressively decreasing with depth up to becoming null for a depth from the rod surface of about 1 mm (Fig. 7).

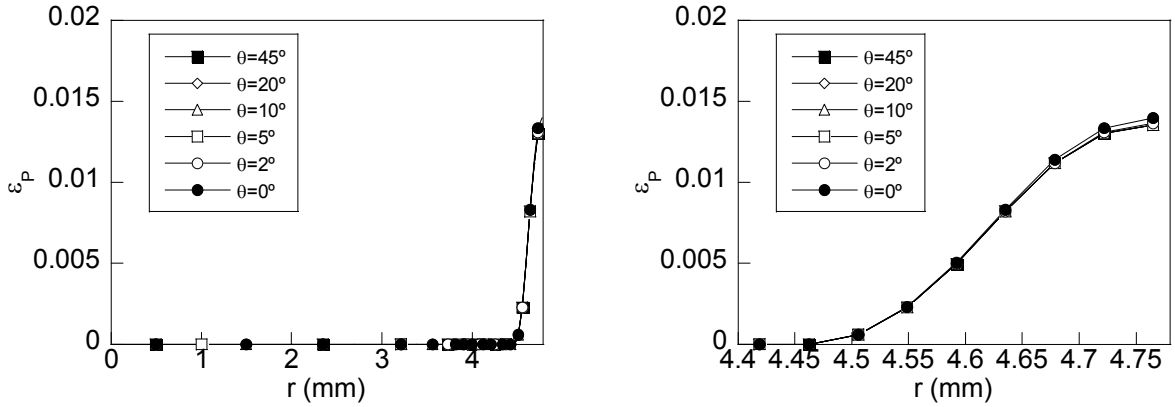

(a) (b)

Figure 5: Radial distribution of equivalent plastic strain for diverse circumferential coordinate θ: (a) general plot and (b) detail plot near the rod surface (zone with strong gradients).

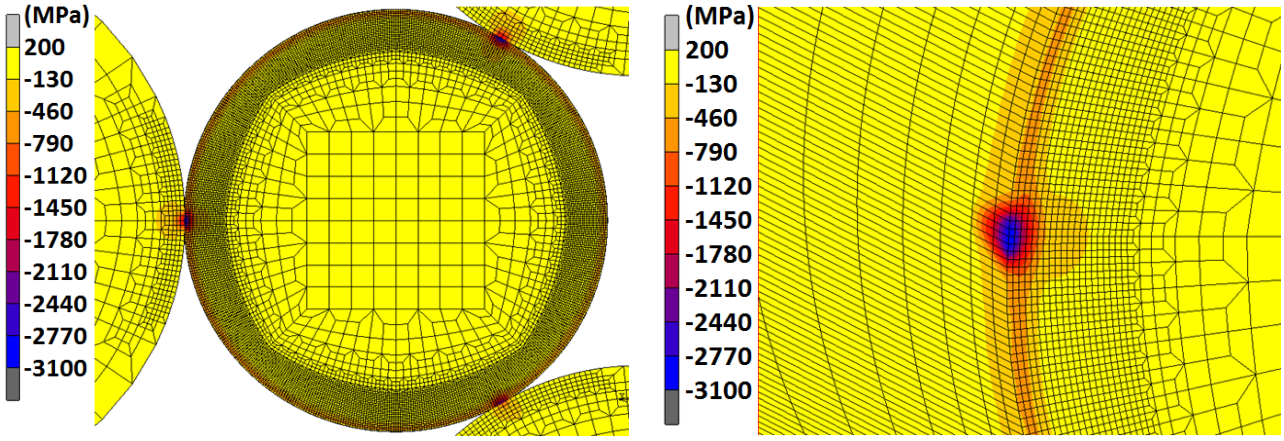

(a) (b)

Figure 6: Distribution of the hydrostatic stress after the sixth loading cycle: (a) 2D view of the contacting plane and (b) 3D view.

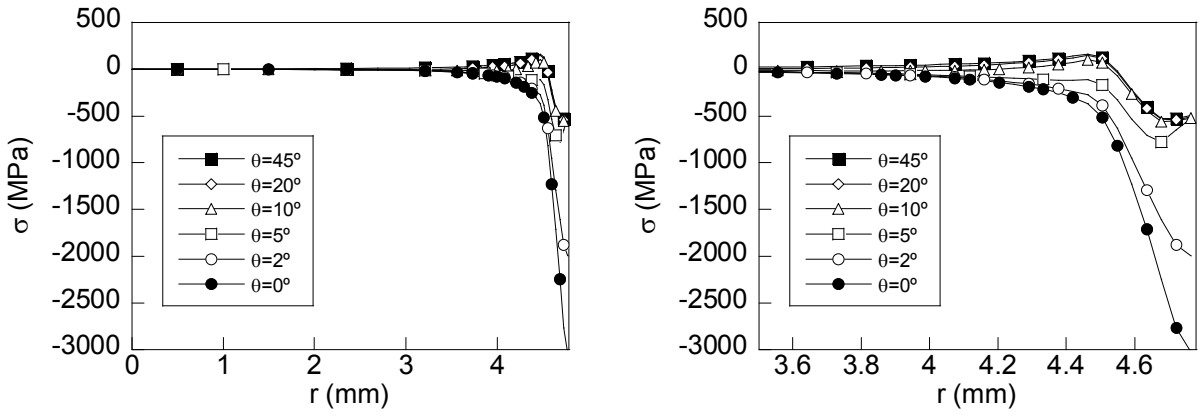

(a) (b)

Figure 7: Radial distribution of the hydrostatic stress for diverse circumferential coordinate θ: (a) general plot and (b) detail plot near the rod surface (zone with strong gradients).

Finally, Fig. 8 shows the axial distribution of both hydrostatic stress and equivalent plastic strain for diverse values of depth from the rod surface (x).

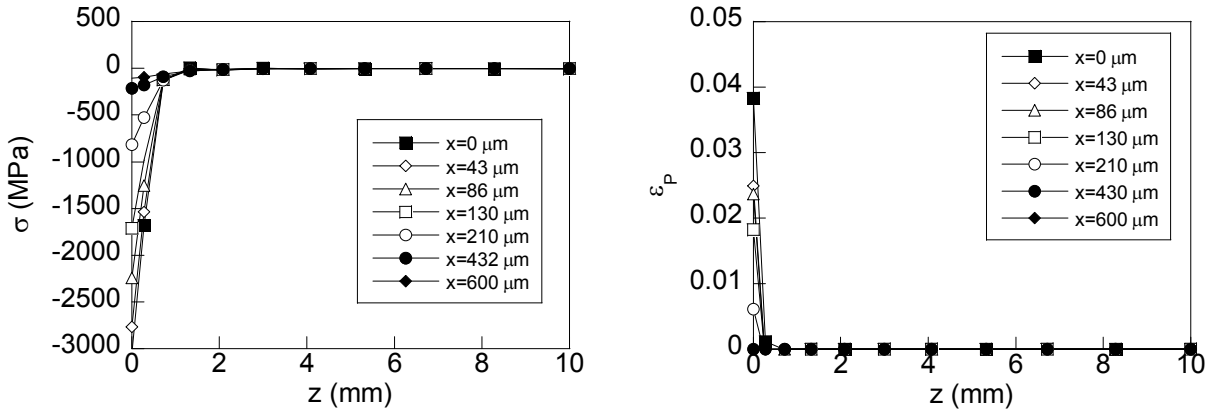

(a) (b)

Figure 8: Axial distribution of the hydrostatic stress for diverse depths (x): (a) general plot and (b) detail plot near the rod surface (zone with strong gradients).

In the axial direction, a very located distribution of both hydrostatic stress and plastic strains near the contact plane is obtained. With regard to the hydrostatic stress distribution, the high compressive stress at the contact plane is progressively decreased as the distance from the contact plane (z) is increased, obtaining a null distribution of such a variable for $z > 1.5$ mm. As the depth from the rod surface increases, the hydrostatic stress at the contacting plane ($z = 0$) progressively decreases and, consequently, the inwards gradient of hydrostatic stress in the axial direction is reduced as the depth from the rod surface is increased. Thus, hydrogen placed close to the contact between ball and bar is also pumped in the axial direction due to the positive inwards gradient of hydrostatic stress. This effect is progressively reduced with the depth x becoming almost negligible for depths $x > 600$ μm. Finally, the axial distribution of plastic strains appears through a narrow zone becoming null for axial distances $z > 500$ μm.

As in the case of the hydrostatic stress distribution, the distribution of plastic strain at the contact plane ($z = 0$) decreases with depth from the rod surface (x), and consequently the inwards gradient is progressively reduced as the variable x is increased, becoming null for depths $x > 600$ μm. However, the inwards gradient of equivalent plastic strains is negative, and so the hydrogen diffusion is not enhanced. This opposition is progressively nullified as the depth from rod surface is increased. So, two competitive factors are involved in the diffusion of hydrogen placed near to the contact between ball and bar. On one hand, the inwards gradient of hydrostatic stress enhances the diffusion of hydrogen out of the contact plane whereas, on the other hand, the inwards gradient of equivalent plastic strain is opposite, thereby impeding the aforesaid diffusion. This effect is very localized near the contact zone and, therefore, the diffusion of hydrogen placed at deeper points ($x > 600$ μm) can be considered null in the axial direction.

CHEMICAL ANALYSIS: HYDROGEN TRANSPORT BY DIFFUSION

For assessing the HE of the rolling rod, it is interesting to analyse the long-time behaviour of the component under hydrogen exposure. To this end, the steady state distribution of hydrogen concentration through the rod radius was obtained (Fig. 9) using Eq. (3) and taking into account both hydrostatic stress and equivalent plastic strain. Plot is associated with infinite time (steady state solution from the mathematical point of view) or with thermodynamical equilibrium of the hydrogen-metal system (from the physical view point).

According to these results, for long time of exposure to the hydrogenating environment, the hydrogen amount at the rod surface vicinity (within the stress and strain affected zone of the rod, i.e., for depths from the rod surface lower than 1 mm) is progressively increased with the circumferential distance to the contacting ball. Therefore, for the plane where the ball is contacting the rod, a huge reduction of the hydrogen amount is observed due to the high compressive stresses produced by the contact pressure that promote hydrogen movement out of the contact affected zone due to the negative

gradient of both driving forces for hydrogen diffusion: the inwards gradient of plastic strain and the inwards gradient of hydrostatic stress.

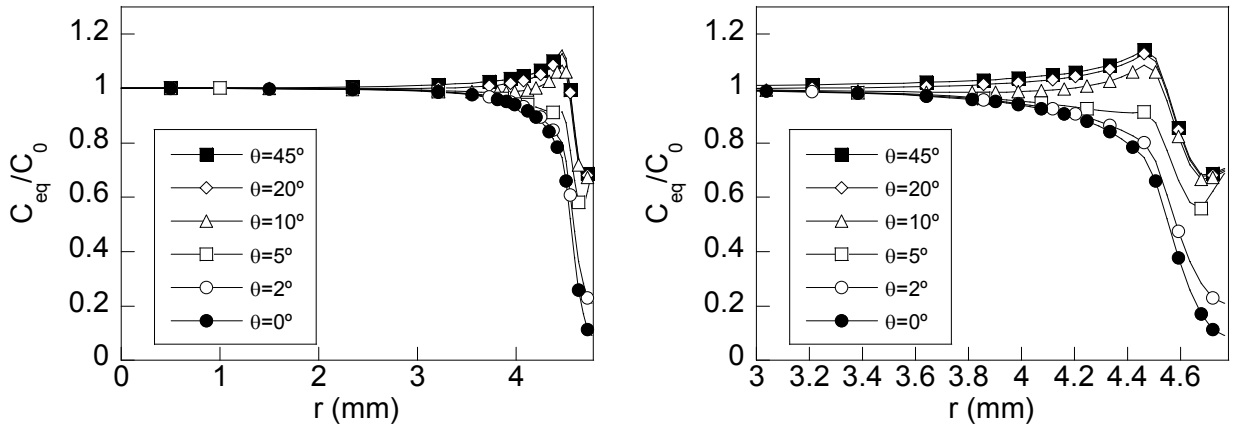

Figure 9: Radial distribution of the hydrogen concentration for diverse circumferential coordinate θ: (a) general plot and (b) detail plot near the rod surface.

Conclusion

In a ball-on-rod test, non-uniform plastic strains are generated on the contact plane where the ball applies a huge pressure to the rod, thus overcoming material yield strength. This state is located near the rod surface with a plastic zone spreading over a maximum depth of 300 μm. A huge compressive stress appears in the vicinity of the rod surface; it is progressively reduced as the distance from the surface increases in radial direction. As a result, hydrogen is accumulated out of the contact plane where a huge reduction of the hydrogen amount is achieved for long times of exposure to the environment due to the high compressive hydrostatic stress in the radial direction, thereby pumping hydrogen towards points outside the contact plane. The maximum hydrogen amount appears for a depth from the surface about 250 μm.

Acknowledgements

The authors acknowledge the financial support provided by the EU Project MultiHy (http://multihy.eu): Multiscale modelling of hydrogen embrittlement of crystalline materials (EU-FP7-NMP Project No. 263335).

References

[1] Europe's onshore and offshore wind energy potential: an assessment of environmental and economic constraints. European Environment Agency, Copenhagen, (2009).
[2] Kumar, A., Hahn, G., Rubin, D., A study of subsurface crack initiation produced by rolling contact fatigue, Metall. Trans. A, 24 (1993) 351–359.
[3] Bhargava, V., Hahn, G. T., Rubin, C. A., Rolling contact deformation and microstructural changes in high strength bearing steel, Wear, 133 (1989) 65–71.
[4] Gupta, V., Bastias, P., Hahn, G. T., Rubin, C. A., Elasto-plastic finite-element analysis of 2-D rolling-plus-sliding contact with temperature-dependent bearing steel material properties, Wear, 169 (1993) 251–256.
[5] Jiang, Y., Su, B., Sehitoglu, H., Three-dimensional elastic-plastic stress analysis of rolling contact, J. Tribol., 124 (2002) 699–708.

[6] Kabo, E., Ekberg, A., Fatigue initiation in railway wheels—a numerical study of the influence of defects, Wear, 253 (2002) 26–34.
[7] Kabo, E., Ekberg, A., Material defects in rolling contact fatigue of railway wheels—the influence of defect size, Wear, 258 (2005) 1194–1200.
[8] Rider, R. J., Harvey, S. J., Chandler, H. D., Fatigue and ratcheting interactions, Inter. J. Fatigue, 17 (1995) 507–511.
[9] Lim, C.B., Kim, K. S., Seong, J. B., Ratcheting and fatigue behavior of a copper alloy under uniaxial cyclic loading with mean stress, Inter. J. Fatigue, 31 (2009) 501–507.
[10] Pandkar, A. S., Arakere, N., Subhash, G., Microstructure-sensitive accumulation of plastic strain due to ratcheting in bearing steels subject to rolling fatigue, Inter. J. Fatigue, 63 (2014) 191–202.
[11] Glover, D. A ball-rod rolling contact fatigue tester, in: Rolling contact fatigue testing of bearing steels. ASTM STP 771, American Society for Testing and Materials, Baltimore, MD, (1982) 107–124.
[12] Bhattacharyya, A., Subhash, G., Arakere, N., Evolution of subsurface plastic zone due to rolling contact fatigue of M-50 NiL case hardened bearing steel, Inter. J. Fatigue, 59 (2014) 102–113.
[13] Arakere, N. K., Subhash, G., Work hardening response of M50-NiL case hardened bearing steel during shakedown in rolling contact fatigue, Mater. Sci. Tech., 28 (2012) 34–38.
[14] Pilkey, W. D., Formulas for stress, strain, and structural matrices, Second ed., John Wiley & Sons, Inc., Hoboken, NJ, USA, (2008).
[15] Toribio, J., Lorenzo, M., Vergara, D., Kharin, V., Hydrogen degradation of cold-drawn wires: a numerical analysis of drawing-induced residual stresses and strains, Corros., 67 (2011) 075001–075008.
[16] Toribio, J., Kharin, V., Lorenzo, M., Vergara, D., Role of drawing-induced residual stresses and strains in the hydrogen embrittlement susceptibility of prestressing steels, Corros. Sci., 53 (2011) 3346–3355.
[17] Toribio, J., Kharin, V., Vergara, D., Lorenzo, M., Two-dimensional numerical modelling of hydrogen diffusion in metals assisted by both stress and strain, Adv. Mater. Res., 138 (2010) 117–126.